



Nanosecond laser-irradiation assisted the improvement of structural, optical and thermal properties of polyvinyl pyrrolidone/ carboxymethyl cellulose blend filled with gold nanoparticles

M. A. Morsi¹ · A. Rajeh² · A. A. Menazea³

Received: 4 September 2018 / Accepted: 10 December 2018 / Published online: 12 December 2018
© Springer Science+Business Media, LLC, part of Springer Nature 2018

Abstract

Gold nanoparticles (Au NPs) supported within the polymeric matrix of polyvinyl pyrrolidone/carboxymethyl cellulose (PVP/CMC) were successfully prepared through the novel in situ method. These (PVP/CMC)/Au hybrid nanocomposites were exposed to nanosecond laser-irradiation with different powers. These nanocomposite samples were investigated before and after the irradiation process through various techniques such as X-ray diffraction analysis (XRD), Fourier transform infrared spectroscopy (FT-IR), ultraviolet/visible spectroscopy (UV/Vis), transmission electron microscope (TEM), differential thermal analysis (DTA) and thermogravimetric analysis (TGA) techniques. The XRD analysis depicted the amorphous nature for PVP/CMC blend and showed the characterizing peaks of Au NPs for the nanocomposite spectrum, where the intensity of these peaks was largely decreased after irradiation process. The FT-IR spectra showed that the blend components were miscible via showing the functional groups of two polymers that were interacted through the formation of a hydrogen bond and the FT-IR spectra of nanocomposite and irradiated samples were affected. Also, the mechanism of interactions between blend and Au NPs was proposed. The UV/Vis. spectra depicted the formation of Au NPs within the PVP/CMC matrix through showing the surface plasmon resonance peak (SPR) of Au NPs at 546 nm. The UV/Vis. the absorbance of this peak was increased and its position was red-shifted after the irradiation process implying the formation of smaller NPs and the narrow size distribution as confirmed by TEM micrographs. The thermal properties for prepared samples were determined through DTA and TGA techniques.

1 Introduction

Nowadays, nanoparticles have a great interest due to its wide range for applications in fundamental sciences, (such as biology, chemistry, and physics), and applied sciences, (like developing and designing the set of nanomaterials based sensors and electronic devices) [1–3]. Au NPs are one the most important classes of noble metal NPs due to their important technological and scientific applications such

as optical sensors, optical switching, color filters and plasmonic/photonic devices [4, 5], where Au NPs advantages are high reactive surface, non-toxicity, strong scattering length, quantum size effect and catalytic properties [5, 6]. Polymer/metal nanocomposites introduce a new alternative for the traditionally filled polymers. These nanocomposites allow both the properties from inorganic NPs and polymer to be combined and therefore new and advanced functions can be induced within the polymeric matrix [1, 7].

Polymer blending is a simple way to have new material with a variety of properties that mainly depend on the characteristics of parent polymers and the composition of blend [6, 8]. The amorphous polymer PVP is chosen due to its individual features such as good thermal stability, non-toxicity and water solubility. Also, it can be thermally cross-linked and can make a set of complexes with various inorganic salts. Furthermore, it is an appropriate reducing/capping agent for NPs because of the existence of (>N– and C=O) groups that do anchoring of NPs at their surface via covalent interaction. This assists in the

✉ M. A. Morsi
m.a_morsi@yahoo.com

¹ Engineering Basic Science Department, Faculty of Engineering, Egyptian Russian University, Cairo 11829, Egypt

² Physics Department, Faculty of Science, Sa'adah University, Sa'adah, Yemen

³ Spectroscopy Department, Physics Division, National Research Centre, 33 El-Behouth St., Cairo 12311, Egypt

stabilization of NPs and binds their aggregation [5, 6, 9]. On the other hand, the biodegradable CMC polymer is one of the significant cellulose derivatives and has considerable characteristics like emulsification, water-soluble, suspension, high transparency, very cheap, easily available, bind and inspissation [8, 10]. Thus, it can be utilized in various applications such as electrical elements, coating development, food packing, textures, papermaking and printing [11–13].

The physical properties of polymeric materials can be modified by exposing different irradiation techniques [5, 6, 14]. These induced modifications are because of the formation of cross-linking and/or chain scissions that prevent the aggregation of NPs as well as to improve their dispersion within the polymeric matrix. Thus, exposing the polymeric materials to laser radiation is one favorable technique to have metal colloids, where the preparation of well-defined NPs is still a considerable challenge towards the effective application for nanostructured systems [15]. This process is a simple low-cost method compared to other physical and chemical methods the fabrication of NPs and introduces the very essential advantage for biological application to synthesis NPs. Preparation of noble metals (Au, silver Ag and platinum Pt), ceramic and semiconductor NPs via laser ablation of metal targets were reported through many studies [15–19].

In this work, we have introduced a novel method to prepare (PVP/CMC)/Au nanocomposite hybrid materials through in situ approach which is set up on the seeded growth for Au NPs within the PVP/CMC blend. Then, we utilize the nanosecond-laser irradiation with different power values to initiate directly the growth for Au NPs on the backbone of the polymer blend and increase their dispersions. Therefore, the concentration of NPs within the nanocomposite can be controlled through varying the power of the laser irradiation process. All samples were characterized using UV/Vis, TEM, XRD, FT-IR, DTA, and TGA techniques.

2 Experimental

2.1 Materials

PVP ($M_w = 72,000$ g/mol, SICO Research Laboratories Pvt. Ltd, Mumbai, India), CMC ($M_w = 250,000$ g/mol, BDH Chemical Advantec Toyoroshi, Japan) and gold chloride trihydrate ($\text{HAuCl}_4 \cdot 3\text{H}_2\text{O}$ 99.9%, Sigma Aldrich, Saint Louis, USA) were used as the raw materials to prepare the nanocomposite samples. Double distilled water (DD) (El-gomhouria Company, Mansoura, Egypt) was used as a common solvent.

2.2 Synthesis of PVP/CMC/Au nanocomposites

The solution casting method was used to prepare the nanocomposite samples. The two polymers were dissolved in the (DD) separately. The two polymers solutions with certain quantity (50/50 wt%) were mixed and stirred for 6 h at 40 °C to obtain a homogeneous solution. Then, 2 ml of HAuCl_4 solution (5 mM) was added to the solution of blend with continuous stirring at pH 6 at 40 °C for 2 h. The color of the mixture was changed from transparent to pinkish-red color implying the formation of Au NPs within the solution of PVP/CMC matrix. The nanocomposite solution was put in ultrasonic for 15 min to increase suspension of Au NPs. Finally, all prepared solutions (virgin polymers, pure blend, and nanocomposite) were poured on to Petri-dishes that was put in an oven at 50 °C to evaporate the solvent and peeled off after 48 h.

2.3 Laser-irradiation process

The samples were irradiated by nanosecond (ns) laser system Neodymium-doped Yttrium Aluminum Garnet (Nd:YAG laser). It is a Q-switched solid-state laser, which producing pulsed nanosecond laser (Continuum laser, Electro-Optics, Inc. Model: PR11 8000, San Jose, CA, USA). The samples irradiated with a second harmonic generation (532 nm). The laser pulses of about 8 ns duration were delivered with a 10 Hz repetition rate and the time of radiation is 3 min. The laser power was varied as listed in Table 1. The distance between the laser source and the samples was 30 cm. The incident laser beam was perpendicular to the samples using quartz concave lens of focal length 100 mm.

2.4 Measurements

The X-ray pattern was recorded on a X'Pert PROXRD analyzer (Malvern Panalytical Ltd. Company, Royston, United Kingdom) with filtered $\text{CuK}\alpha$ radiation ($\lambda = 1.540 \text{ \AA}$) working at 30 kV acceleration and 10 mA current of the X-ray

Table 1 The notations of prepared/irradiated samples and grain size

Sample	Sample notation	Irradiation power (mW)	Grain size (nm)
Pure blend PVP/CMC	Pure blend	0	–
(PVP/CMC) blend/Au nanocomposite	S0	0	39
	S1	167	35
	S2	270	33
	S3	570	23
	S4	670	15

tube, scan step was $0.05^\circ \text{ min}^{-1}$ and 1 s acquisition time. FT-IR spectra were recorded on Nicolet iS10 FT-IR spectrometer (Thermo Fisher Scientific company, Waltham, MA USA) having a resolution 4 cm^{-1} in the wave number range from 400 to 4000 cm^{-1} to examine their structure. ChemDraw Software (Cambridge Soft Corporation, USA) was utilized to draw the molecular schemes. The UV/Vis absorption spectra of polymer films were recorded using spectrophotometer (V-570 UV/VIS/NIR, JASCO INC., Easton, USA), in the wavelength range 200 – 1000 nm . Transmission electron microscopy (TEM) image was scanned on a JEOL 1200 EX instrument, Tokyo, Japan operating at an accelerated voltage of 120 kV . Energy dispersive X-ray spectroscopic analysis (EDX) spectroscopy was measured on SEM instrument (JEOLJSM 6510 LV) (JEOL Company, Tokyo, Japan) equipped with an Oxford EDAX system. The thermal measurements were performed for the different films using the DTA-50 instrument (Shimadzu Company, Kyoto, Japan) in the temperature range [room temperature (RT)– 450°C] with a heating rate of 10°C/min in a nitrogen atmosphere. The weight loss was obtained for the prepared samples by TGA thermal analyzer (STD-Q600) (TA Instruments Company, New Castle, DE USA) at a heating rate 5°C/min from RT to 500°C in a nitrogen atmosphere.

3 Results and discussion

3.1 XRD technique

XRD technique is the most common analysis tool to depict the Au NPs formation and to know the crystal particle size and the crystalline phase present. The XRD patterns for pure PVP, pure CMC, and pure PVP/CMC blend are shown in Fig. 1 while Fig. 2 shows the XRD patterns of pure PVP/CMC blend and nanocomposite sample before and after laser-irradiation with different powers. The XRD spectra for both PVP and CMC polymers confirm their semicrystalline nature. The CMC spectrum shows a broad peak at $2\theta = 21.64^\circ$ [12, 20]. The pure PVP film is characterized by two halos centered at $2\theta = 10$ and 22.50° [6, 21]. Thus, the XRD spectrum for pure PVP/CMC blend is also semicrystalline with the main halo peak at 22.80° .

Upon HAuCl_4 embedding within PVP/CMC matrix, additional peaks appear and there are observable variations in the intensity for XRD peaks of the filled sample (nanocomposite sample) as in Fig. 2. In addition to the main halo peak at $2\theta = 22.80^\circ$ for the nanocomposite spectrum, it exhibits a small halo peak at $2\theta = 10^\circ$. This is the characteristic peak for PVP of the nanocomposite sample. New diffraction peaks at $2\theta = 38.01^\circ$ (111), 44.37° (200), 64.59° (220) and 77.65° (311) indicate the face center cubic (FCC) for Au NPs (JCPDS File No. 4-0784) [6, 22]. This

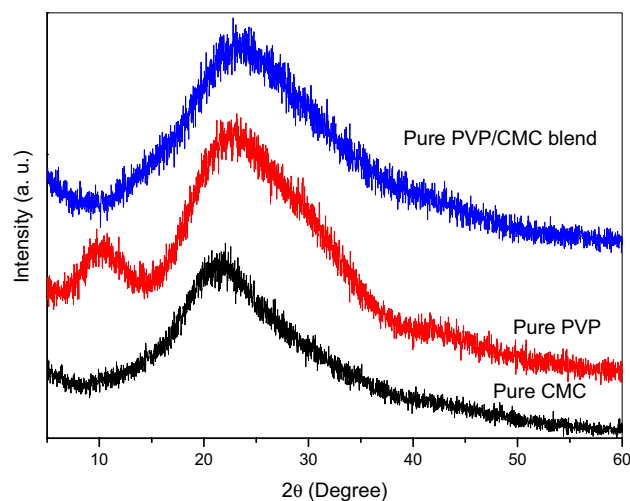


Fig. 1 XRD spectra for pure CMC, pure PVP and pure PVP/CMC blend (50/50 wt%)

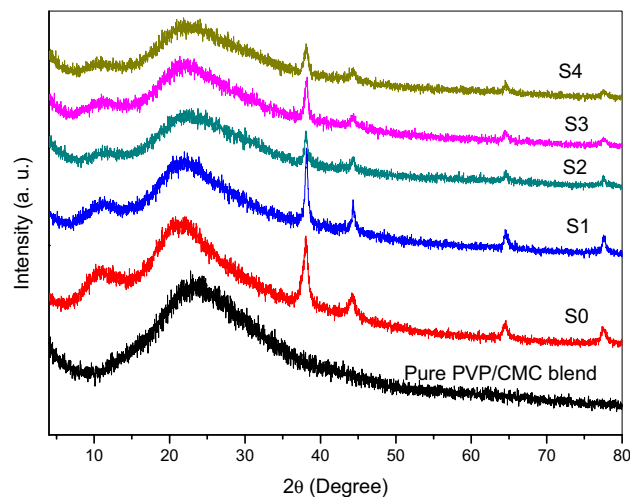


Fig. 2 XRD spectra for pure blend and its nanocomposite sample before and after laser-irradiation at different powers

observation depicts that the Au NPs are successfully in situ prepared within PVP/CMC matrix due to the interaction between HAuCl_4 and the functional groups of blend components [23], carbonyl group (C=O) of PVP and the carboxylate group (COO^-) of CMC, that behave as stabilizer and polyol-reductant respectively. Also, this interaction is confirmed by shifting in the position of the main amorphous peak at $2\theta = 22.80^\circ$ to lower angle $2\theta = 21.90^\circ$ and reduction in the intensity of XRD pattern for the nanocomposite sample which implies that the content of amorphous regions is increased within the polymeric matrix of nanocomposite sample [6, 24]. This shift points out that the HAuCl_4 addition seems to alter weakly the average inter-segmental spacing of polymer chains [25, 26]. Moreover, it depicts that the

complexation between PVP/CMC matrix and HAuCl_4 exists in the amorphous region.

Second, as the power of the laser-irradiation process increases from S1 to S4, the intensity for the main peak and Au lines reduces and broadens progressively in accordance with their small grain sizes. These observations imply that the nanocrystals have lesser lattice planes compared to bulk. This indicates that the laser-irradiation process with high power induces an increase for the content of amorphous regions because of the formation of free radical, as a result from bond cleavage, hydrogen elimination and/or chain scission, that may lead to the formation of cross-linking for the polymeric matrix by recombination reaction, other side reactions such as double bond formation and a reduction for the molecular weight of the polymeric matrix for irradiated samples. The slight increase for the broadness and the reduction in the intensity of diffraction peaks indicate the decrease in the Au NPs size. Abd El-Kader et al. [15] found that the XRD intensity of Ag NPs peaks within poly (*n*-vinylcarbazole) (PVK) was largely decreased as the laser pulse power was increased from 140 to 570 mW. Debye-Scherrer's formula is used to calculate the average grain size for NPs at $2\theta = 38.01^\circ$ with (111) planes and the obtained calculations are listed in Table 1. It can be observed that the NPs size decreases with increasing the power of the irradiation process.

3.2 FT-IR spectroscopy

FT-IR spectroscopy is performed to manifest the interactions between the functional groups of PVP/CMC blend and HAuCl_4 and the laser-irradiation effects. The FT-IR spectra for virgin polymers (pure PVP and pure CMC) and pure PVP/CMC blend (50/50 wt%) are shown in Fig. 3 while Fig. 4 shows the FT-IR spectra of the nanocomposite sample before and after the laser-irradiation process with different powers. Table 2 lists the functional groups for the pure polymers and their assignments [9, 12, 13, 20, 21, 27–31].

From Fig. 3, the spectrum for pure blend sample contains both carbonyl group ($\text{C}=\text{O}$) of PVP at 1660 cm^{-1} and the [carboxylate (COO^-) and ($\text{CH}_2-\text{O}-\text{CH}_2$)] groups of CMC at 1600 and 1060 cm^{-1} . The existence of these groups implies that the PVP/CMC components are miscible and are interacted together via hydrogen bond formation (Scheme 1). This interaction is confirmed by the decrease in the OH absorbance of a blend and an increase for the broadness of $\text{C}=\text{O}$ group. The absorbance for COO^- group is largely reduced and is overlapped with the $\text{C}=\text{O}$ group and appeared as a shoulder. Also, the absorbance for $\text{CH}_2-\text{O}-\text{CH}_2$ and OH bending group is decreased.

For the spectrum of nanocomposite sample S0, filling process with HAuCl_4 induces effects and changes on the functional groups of PVP/CMC matrix. It is observed that

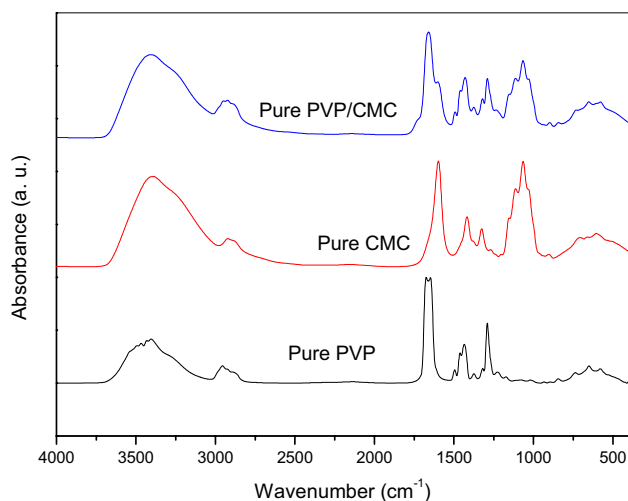


Fig. 3 FT-IR spectra for pure PVP, pure CMC and pure PVP/CMC blend

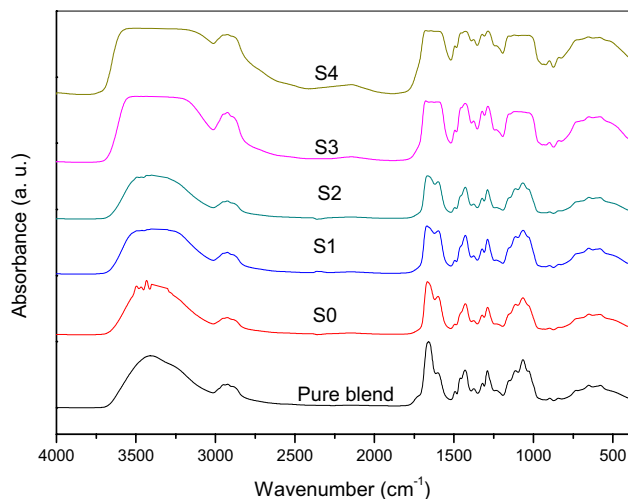
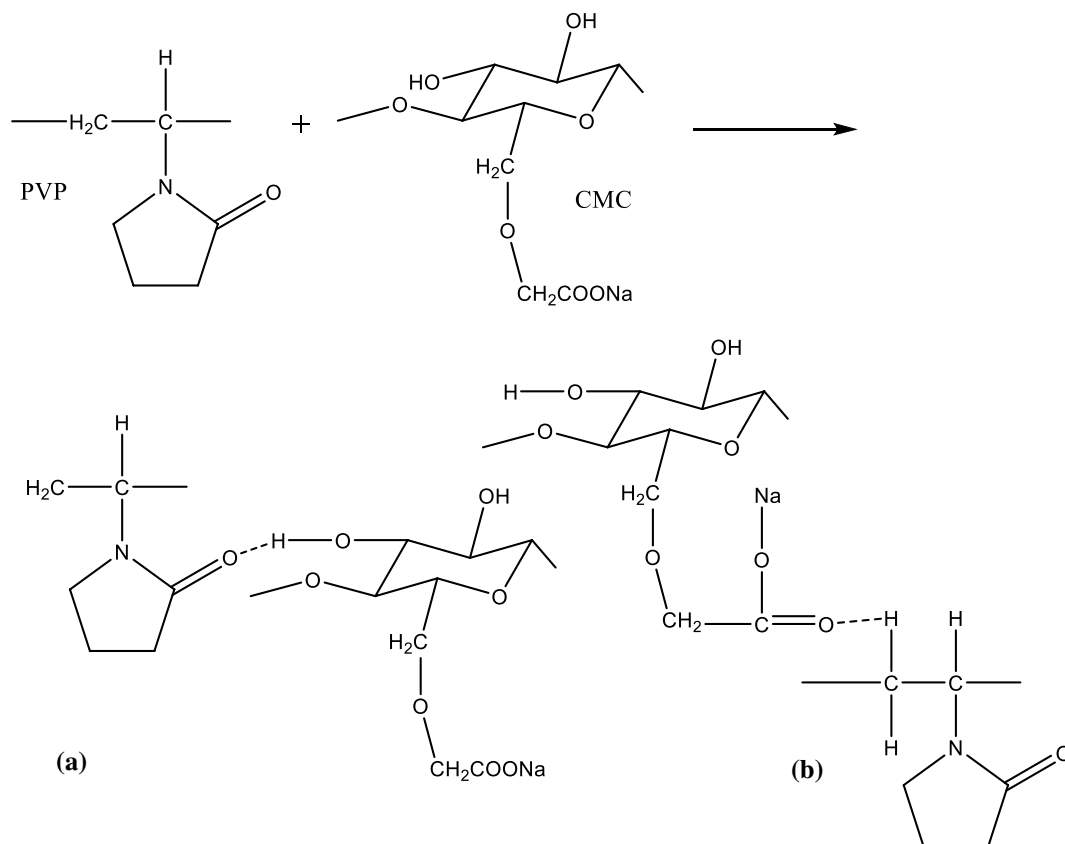


Fig. 4 FT-IR spectra for pure PVP/CMC blend and (PVP/CMC)/Au nanocomposite before and after laser irradiation at different powers

the FT-IR spectrum for S0 sample is almost identical to the corresponding spectrum of PVP/CMC blend. But, it is worthwhile to pay attention to the structural features existed in the wavenumber range $1750\text{--}950\text{ cm}^{-1}$. The absorbance of the functional groups in this wavenumber region is decreased. The features of bands at 1660 , 1600 , 1290 and 1060 cm^{-1} are changed. Also, the intensity of absorption peaks at 1495 and 1460 cm^{-1} are largely decreased. These results depict that there is an interaction between the components of PVP/CMC blend and HAuCl_4 (Schemes 2 and 3), which results in a reduction of Au ions and formation of Au NPs. A PVP macromolecule may contribute in some forms for interaction/association with

Table 2 Assignments of the FT-IR characterization bands of the pure CMC and pure PVP

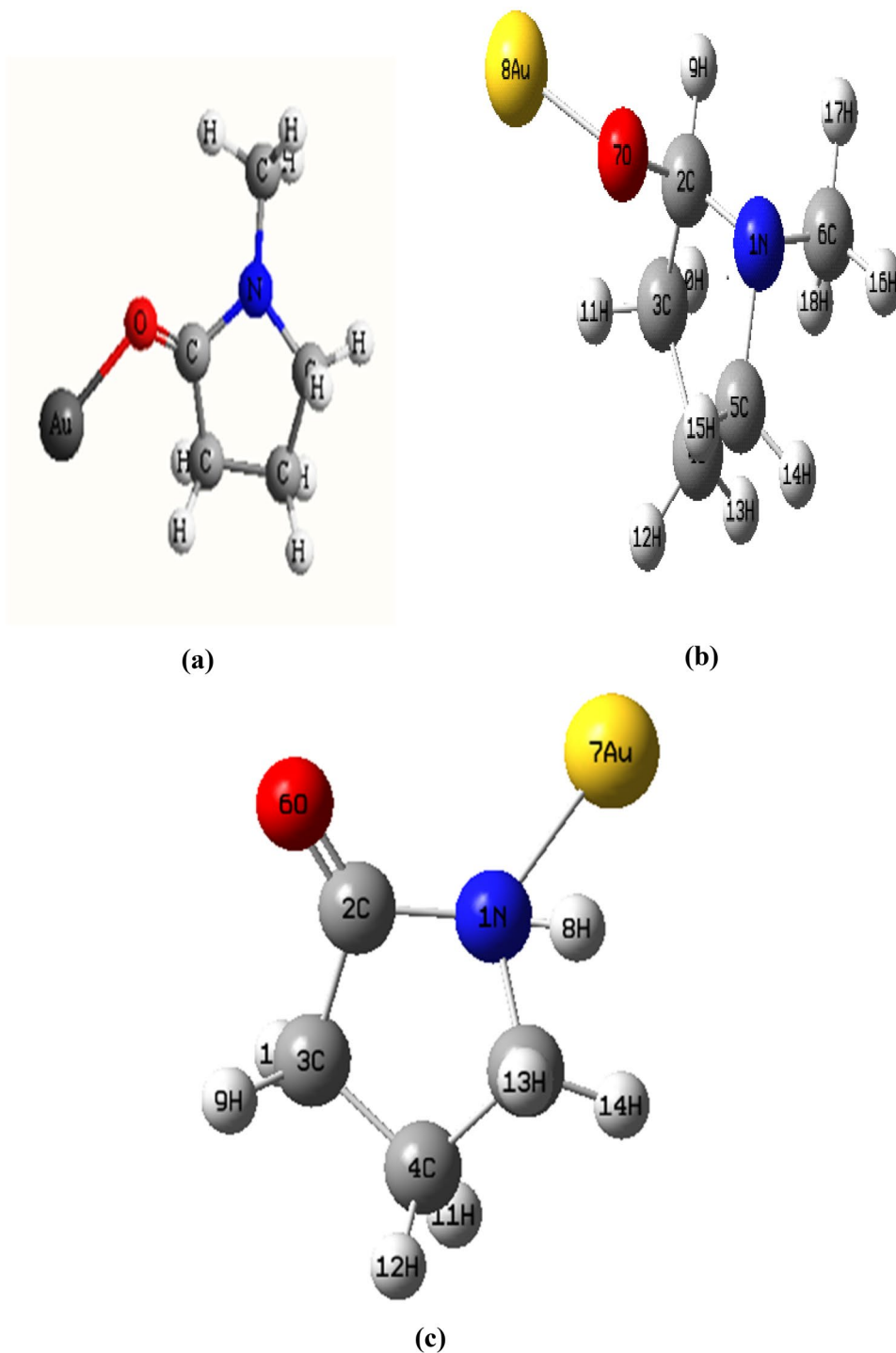
Pure CMC		Pure PVP	
Wavenumber (cm ⁻¹)	Assignment	Wavenumber (cm ⁻¹)	Assignment
3401	OH stretching	3425	OH stretching
2890	CH ₂ asymmetric stretching	2955	CH ₂ asymmetric stretching
1600	COO ⁻ group	1660	Symmetric and asymmetric of C=O
1419	CH ₂ scissoring	1495	Vibration of C=N (pyridine ring)
1322	OH bending	1460	C–H bending of CH ₂ or OH bending
1060	CH ₂ –O–CH ₂ stretching	1435	CH ₂ wagging
–	–	1375	Swinging vibration of C–H in CH ₂ group
–	–	1290, 1230	CH ₂ (wagging or twisting) or N–OH complex
–	–	1172, 845	C–C stretching
–	–	737	Out-of-plane rings C–H bending/C–N stretching vibration
–	–	650	C–N bending

**Scheme 1** Mechanism of hydrogen bond formation between PVP and CMC monomers

the gold ions and reduces these ions into metallic NPs. The interaction, (i.e. formation of ionic and coordination bonds), between PVP/CMC and metal NPs, may exist by the adsorption of pyrrolidone ring/CH₂COONa on the surface of metal nanoparticles by;

- Nonbonding electrons of a carbonyl group of PVP and –COONa of CMC [10, 23].
- Adsorption of pyrrolidone of PVP via a Nitrogen atom.
- Adsorption via both carbonyl group and Nitrogen atom [23].

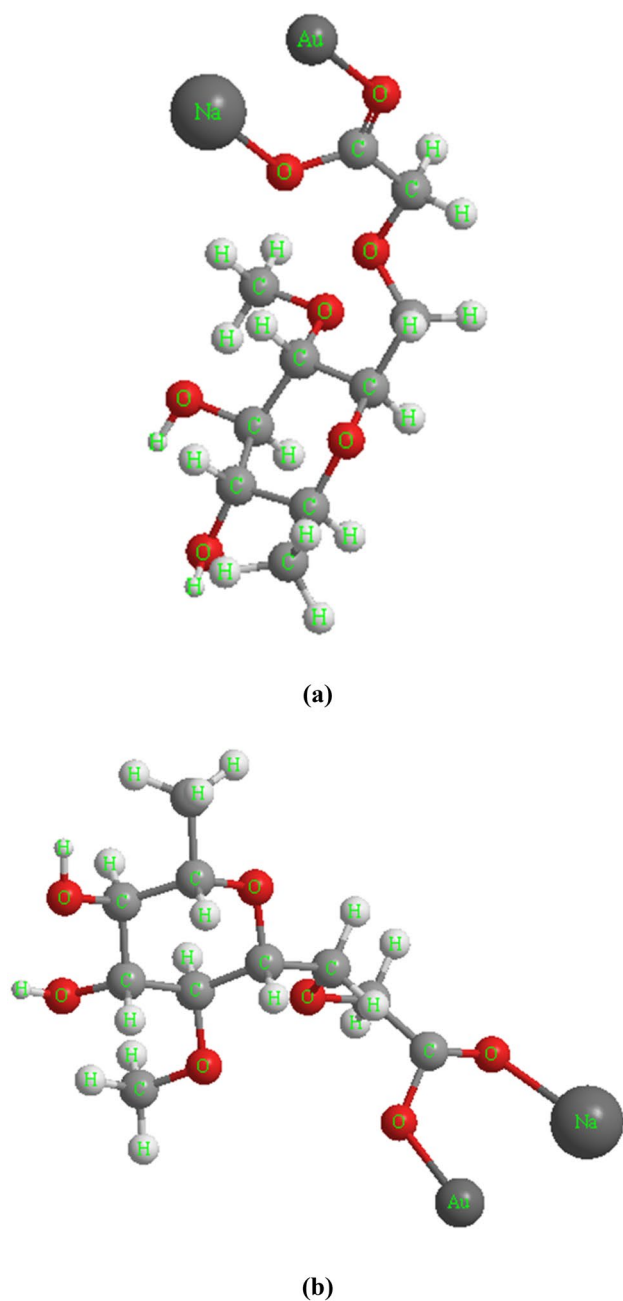
Scheme 2 The structure of the possible modes for the interaction between PVP and Au [23]



The PVP unit composes of an amide group where O and N atoms of this polar group probably have a strong affinity for the gold ions [9, 32]. While CMC macromolecules are a reducing agent for gold ions and stabilizing agent for the formed Au NPs because it composes of chemically modified cellulose chains containing carboxyl groups. The negatively charged COO^- groups attract the positively charged Au cations [33, 34]. All these components with their reducing

properties support the utilization of PVP/CMC matrix as reducing and stabilizing agent for the Au NPs synthesis.

For irradiated samples, the FT-IR spectra show that the broadness of OH stretching is increased and the absorbance of CH_2 asymmetric stretching is increased. The features of the main functional groups in $1750\text{--}950\text{ cm}^{-1}$ region, like ($\text{C}=\text{O}$, COO^- and $\text{CH}_2\text{--O--CH}_2$) groups,



Scheme 3 The structure for the possible interactions of Au with CMC monomer

are gradually affected and diminished with continuous increasing the power of laser-irradiation process. Also, the absorbance of these peaks is increased accompanied with an increase for its broadness. These results occur because of the formation of chain scission/cross-linking via irradiation process that results into an increase for the amorphous region contained within the irradiated samples as confirmed by XRD analysis.

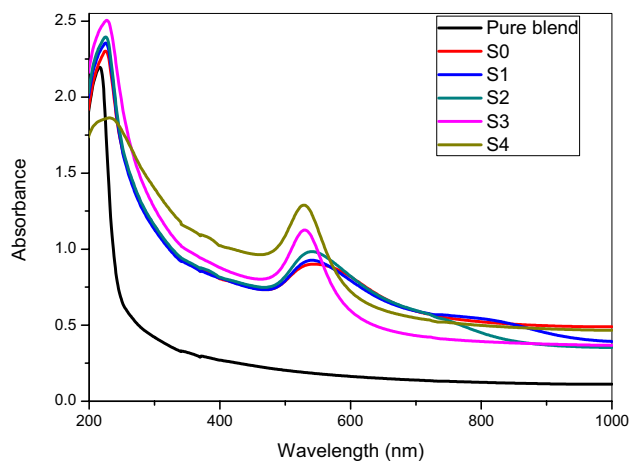


Fig. 5 UV/Vis spectra for pure PVP/CMC blend and blend/Au nano-composites irradiated with different laser-irradiation powers

3.3 UV/Vis spectroscopy

Figure 5 shows the UV/Vis absorption spectra for the prepared samples. The spectrum of pure PVP/CMC sample has the absorption peak at 216 nm, which is attributed to $n \rightarrow \pi^*$ [6], and exhibits a sharp absorption edge that has a sharp decrease with increasing the wavelength and is red shifted toward longer wavelengths for the S0 sample. This shift is occurred because of the variation in the content of amorphous phase within S0 matrix, as depicted by XRD results, that leads to a change in the values of the optical energy gap and refractive index [5, 6, 21, 35]. Also, the spectrum of the S0 sample shows a new peak in the visible region at 546 nm. This peak is attributed the surface plasmon resonance peak (SPR) for Au NPs [4, 5, 22, 36, 37]. The appearance of this broad peak may be indicated to the formation of the small quantity of reduced Au NPs within the PVP/CMC matrix. The spontaneous formation for Au NPs can be attributed to the direct redox between PVP/CMC and Au ions since there is no other reducing agent in the system. The enhancement for absorbance is in agreement with the color change for the S0 sample to a pinkish-red.

For irradiated samples, the sharp absorption edge is red shifted with increasing the power irradiation process from S1 to S4 and the SPR peak position is shifted toward shorter wavelengths, from 546 nm to 528 nm, associated with an increase for its absorbance due to the quantum size effect as a result from the irradiation effects [5, 6]. Abdelghany et al. [6] found that the position of SPR peaks for Au NPs within polyethylene oxide/polyvinyl pyrrolidone (PEO/PVP) blend was shifted from 536 to 529 nm as the dose of the gamma-irradiation process was increased from 3 to 5 Mrad. The increase for the absorbance of SPR peak implies that there is an increase for the Au NPs fraction and its blue shift is related to the generation of smaller particles which will be

confirmed by TEM micrographs. These results are because of induced effects via the laser-irradiation process such as chain scission and cross-linking [38, 39]. These effects, in turn, will increase the molecular mass and the number of polymeric chains surrounding the NPs that inhibit the Au NPs aggregations [40, 41]. Morsi and Abdelghany [5] reported that the absorbance of SPR peak for (PEO/PVP)/Au nanocomposite was increased as the exposure time to UV radiation was increased from 1 to 8 h. Moreover, the increase for the power of the laser-irradiation process will result in an improvement for the rate of nucleation that leads to the formation of smaller particles [4–6, 41]. Also, the SPR peak becomes narrower with increasing the power of the irradiation process. This result indicates that the narrow size distribution for the Au NPs at higher powers is achieved as depicted via the XRD technique.

3.4 TEM and EDX

TEM technique is utilized to have detailed information on the size distribution for NPs within the polymeric matrix before and after the laser irradiation process. Figure 6 shows the TEM images for the S0, S1 and S4 samples with the corresponding size distribution histogram. From the micrograph of S0 sample, the in situ prepared Au NPs are spherical in shape with average size range 1–40 nm. This result is in agreement with the broadness and position of the SPR peak in the UV/Vis spectrum of the S0 sample. This size range is decreased to 1–35 nm for the S1 nanocomposite sample. For S4 nanocomposite sample, the size and shape of NPs are nearly uniform and then the size range is also decreased to 2–20 nm. This indicates that the size of prepared NPs gets smaller and depicts the effective role of the laser-irradiation process with different power values in the monodispersity/distribution of the formed NPs within S4 matrix. Abd Elkader et al. [15] reported that the average size for PVK/Ag nanocomposites at laser power 140, 170 and 570 mW was found to be 44, 34 and 23 nm, respectively. Also, the decrease in the particle size range is in agreement with that calculated earlier in XRD technique and that reported in the literature [15, 42, 43]. These results are confirmed in the UV/Vis spectra of the SPR peak for irradiated samples by the decrease in its broadness, the shifting toward shorter wavelength and an increase for its intensity. Figure 7 demonstrates the diffraction pattern for the prepared Au NPs within S0 sample which shows the characteristic crystal planes of the elemental Au due to its face-centered cubic nature [4, 22, 37]. While, Fig. 8 shows the EDX analysis for the S0 nanocomposite. Elemental gold can be observed at around 2.25, 8.50, 9.75, 11.45 and 13.75 keV [4, 44] in support of the results XRD and UV/Vis techniques that confirmed the existence of Au NPs within the PVP/CMC matrix.

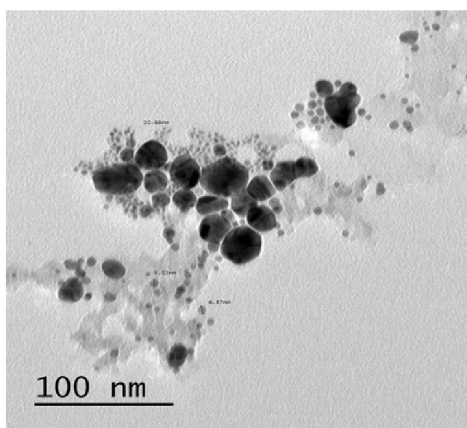
3.5 Thermal properties

On heating the polymeric materials, various thermal phenomena such as a glass transition (T_g), melting (T_m), and decomposition (T_d) temperatures may exist. DTA is one of the most appropriate techniques for studying these phenomena and can be used to study the miscibility for the components of blend [45]. Figure 9 shows the DTA curves for the prepared samples from the RT to 450 °C. The DTA curve for pure PVP/CMC blend shows an endothermic T_g peak at 80 °C. This peak may be because of the overlapping T_g for the two polymers of blend where the T_g values for pure PVP and pure CMC are 90 °C and 75 °C, respectively [5, 6, 46–48]. Also, appearing a single T_g indicates that the components of PVP/CMC blend are miscible and homogeneous. From the DTA curve for the S0 sample, the position of T_g is slightly shifted to 82 °C and this shift toward higher temperatures is largely increased for irradiated samples. This increase may be assigned to the increase of the mean molecular weight of polymer in amorphous region [45] and the segmental mobility of amorphous polymer decreases and becomes more rigid segments because of both the formation of Au NPs within S0 matrix and the induced effects due to irradiation process [5, 6, 14].

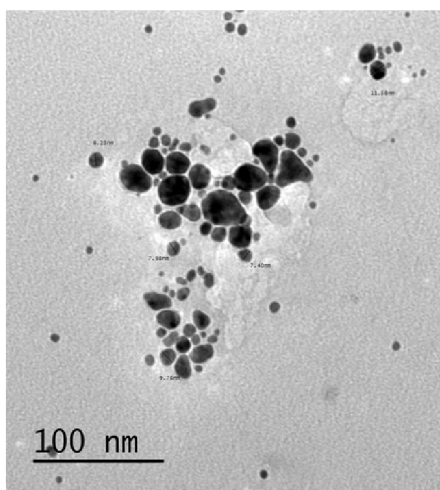
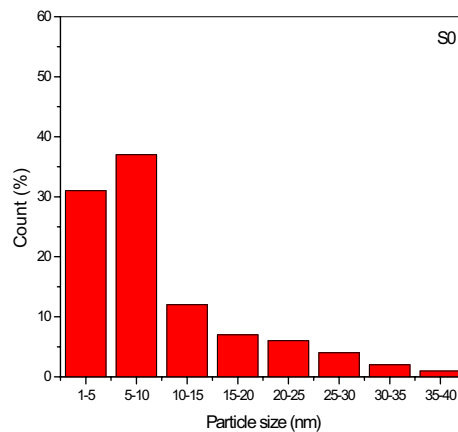
The T_m for the pure blend has appeared as an exothermic peak at 313 °C. The T_m value for PVP/CMC blend is larger than that of pure PVP ($T_m = 190$ °C) [14, 49] and lower than that of pure CMC ($T_m = 320$ °C) [48, 50]. This is as a result of the interaction between PVP and CMC, as confirmed by FT-IR spectroscopy, which in turn decrease the degree of crystallinity. Also, the existence of a single T_m indicated that PVP and CMC had good miscibility [45]. For the S0 and irradiated samples, it has appeared that the position of T_m peak is nearly the same but area under this peak is decreased for S0 sample and is largely decreased for irradiated samples. This area expresses the total heat of fusion for the samples [51, 52]. The decreased heat of fusion should be the effect of lower crystallinity because the content of the amorphous phase is increased. The total heat of fusion for S0 and irradiated samples was lower than for pure blend, likely since both the irradiation effects and the interaction between the formed Au NPs and PVP/CMC interrupt the rearrangement of polymer chains [5, 6, 52].

The T_d for the pure blend has appeared as a broad endothermic peak at 371 °C. The position of this peak is shifted to 398 °C for the S0 sample, indicating the existence of intermolecular interactions between the PVP/CMC and Au NPs. For irradiated samples, the position of T_d peak is shifted to higher temperature values. This observation demonstrates that the laser-irradiation process enhances the thermal stability for S0 samples. This improvement can be due to the increase for the content of disorder regions within the PVP/CMC matrix and the

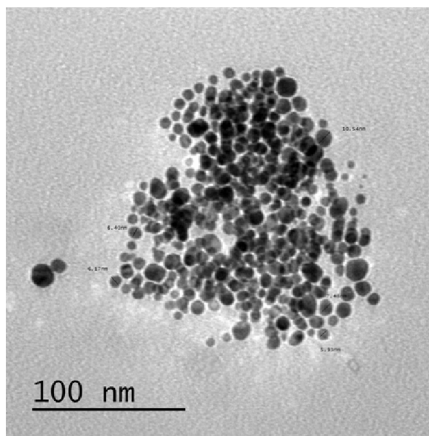
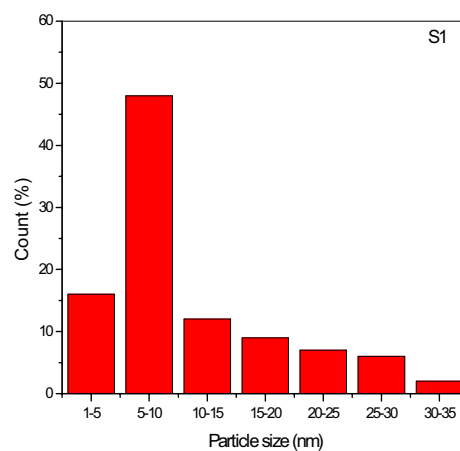
Fig. 6 TEM micrographs for the S0, S1 and S4 nanocomposite samples



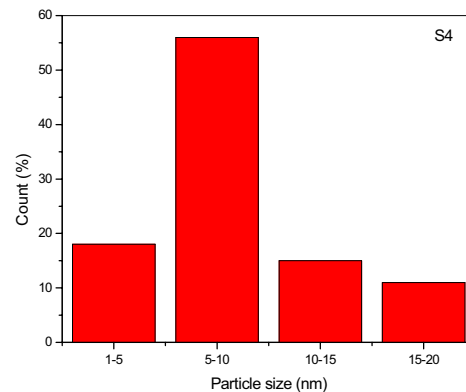
S0 sample



S1 sample



S4 Sample



fine dispersion of Au NPs. The chain-scission reactions and the continual eliminations, as a result from irradiation effects, need more energy and exist at a higher

temperature, where the polymeric chain undergoes a series of thermal decomposition reactions that are able to change its main structure [5].

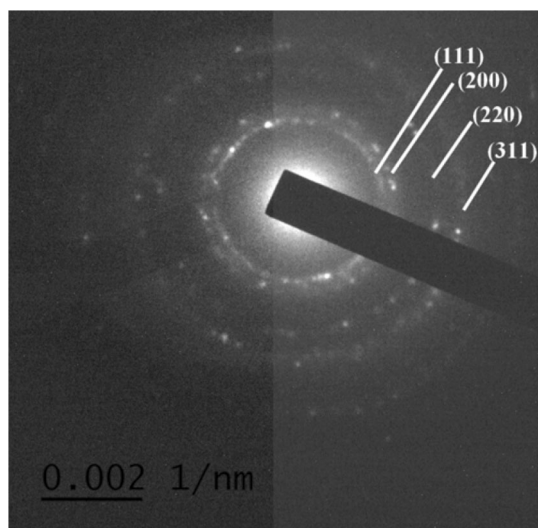


Fig. 7 Electron diffraction pattern for the S0 nanocomposite samples

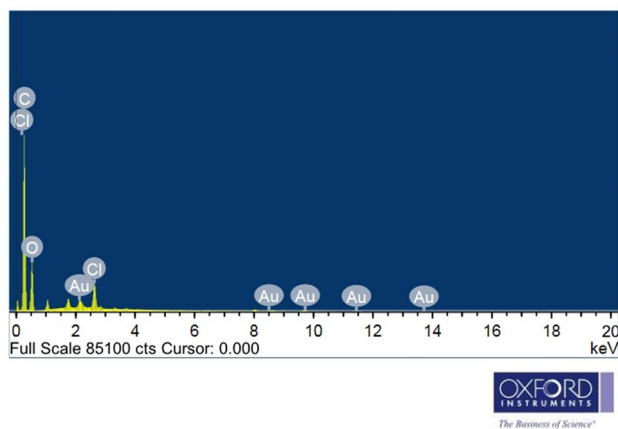


Fig. 8 EDX graph for the S0 sample

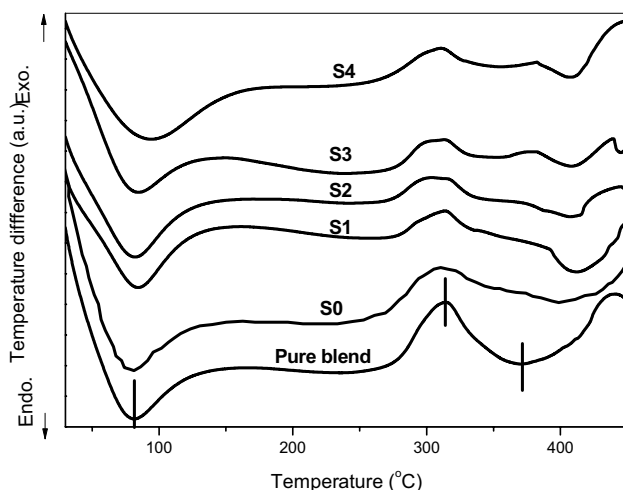


Fig. 9 The DTA curves for the prepared samples

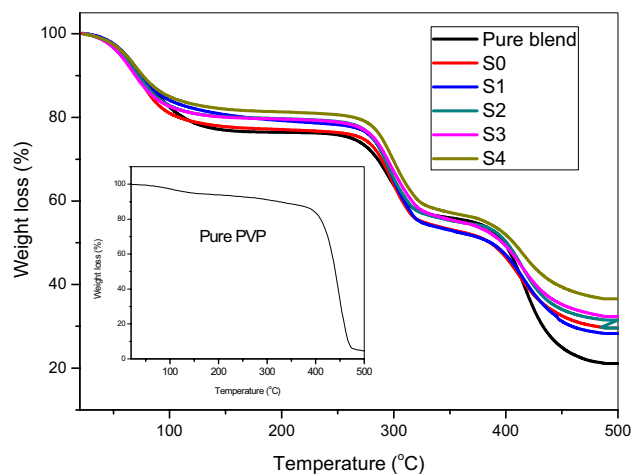


Fig. 10 TGA curves for the prepared samples

Figure 10 shows the TGA thermograms for pure PVP/CMC blend, blend/Au, and irradiated samples. It is obvious that the degradation mechanism is not affected due to HAuCl_4 addition and laser-irradiation process, but the thermal stability is affected. From the TGA curve for PVP/CMC blend, it shows three stages for the degradation. The first stage has occurred in the temperature range 30–150 °C with the weight loss of 22.80%. This stage is indicated to the loss of water within PVP/CMC where the nature of blend components is hygroscopic [53, 54]. For the second stage, a 20.90% of weight loss has existed in the temperature range (250–371 °C) as a result from the CMC degradation where the decomposition, elimination of OH groups, dehydration and ring scission are existed [53]. Su et al. [55] reported that the main weight loss for CMC polymer has arisen from CO_2 from the COO^- groups of CMC. In the temperature region (380–484 °C), the third stage with weight loss 33.42% is existed and leaving a residue of 22.80% above 484 °C. This thermal stage is due to the thermal degradation of PVP as shown in the inset figure. In this stage, the chain-scission reaction and reactions of intermolecular and intramolecular condensation have occurred until the polymer is quite roasted [5, 56].

For the S0 sample, the TGA curve shifts toward higher temperatures as a result of the interaction between the PVP/CMC matrix and Au NPs with a large surface area as confirmed in FT-IR results. This enhancement for the thermal stability of the S0 sample can be referred to the catalysis ability of Au NPs and also their ability in raising the crosslinking density within S0 matrix [57]. The diffusion of degradation products from the bulk polymer to the gas phase is slowed down. Thus, this acts as a heating barrier to protect the PVP/CMC inside and the nanocomposite has a pronounced enhancement in thermal resistance compared to the pure PVP/CMC.

After the laser-irradiation process, the values of degradation temperature increase and the TGA curves moves towards higher temperature values implying the thermal stability improvement for S1, S2, S3, and S4 nanocomposites. This observation indicates the existence of cross-linking and chain-scission as a result of the of irradiation process effects [5, 6]. These induced effects within irradiated samples lower the mobility of chains that will exhaust more heat than the matrix for S0 sample and does not allow the gathering of heat within the latter and consequently inhibits oxidation at the early stages for decomposition. Furthermore, delaying in the degradation process of irradiated samples, especially S3 and S4 nanocomposites, can be due to finer dispersion for Au NPs that behaved as efficient heat sinks [6].

4 Conclusions

An efficient, simple and cost-effective in situ method for preparing highly monodispersed polymer/Au nanocomposite has been developed through incubating gold chloride trihydrate within the polymeric matrix of PVP/CMC blend and then exposed to laser-irradiation process with different values of power. Results of XRD technique confirmed the formation of Au NPs within PVP/CMC matrix through showing their characterizing diffraction peaks at $2\theta = 38.01^\circ$ (111), 44.37° (200), 64.59° (220) and 77.65° (311) and showed that the content of amorphous phases was increased for irradiated samples. FT-IR spectroscopy indicated that both Au NPs and laser-irradiation process were greatly affected on the main polar groups of PVP/CMC blend such as amide and COO^- groups. The UV/Vis absorption spectra indicated that the SPR peak became narrower and the absorbance of this peak was increased with increasing the power of the irradiation process. The size and distributions of Au NPs were enhanced for irradiated nanocomposites with high powers of the laser as confirmed from TEM micrographs. Thermal techniques depicted that the thermal stability of PVP/CMC was improved after embedding HAuCl_4 and the laser-irradiation process. From all previous results, the improved structural, optical and thermal properties for PVP/CMC by the in situ prepared Au NPs and controlling the power of laser-irradiation process will increase its potential applications such as filters, optical coatings, thermal devices, and modern optoelectronics.

Compliance with ethical standards

Conflict of interest The authors declare that they have no conflict of interest.

References

1. M.A. Morsi, S.A. El-Khodary, A. Rajeh, Enhancement of the optical, thermal and electrical properties of PEO/PAM: Li-polymer electrolyte films doped with Ag nanoparticles. *Physica B* **539**, 88–96 (2018)
2. S. Choudhary, R. Sengwa, ZnO nanoparticles dispersed PVA-PVP blend matrix based high-performance flexible nanodielectrics for multifunctional microelectronic devices. *Curr. Appl. Phys.* **18**(9), 1041–1058 (2018)
3. A.M. Abdelghany, M.A. Morsi, A. Abdelrazek, M.T. Ahmed, Role of silica nanoparticles on structural, optical and morphological properties of poly (vinyl chloride-co-vinyl acetate-co-2-hydroxypropyl acrylate) copolymer. *Silicon* **10**, 519–524 (2018)
4. A. Abdelghany, E. Abdelrazek, S. Badr, M. Abdel-Aziz, M. Morsi, Effect of Gamma-irradiation on biosynthesized gold nanoparticles using *Chenopodium murale* leaf extract. *J. Saudi Chem. Soc.* **21**(5), 528–537 (2017)
5. M. Morsi, A. Abdelghany, UV-irradiation assisted control of the structural, optical and thermal properties of PEO/PVP blended gold nanoparticles. *Mater. Chem. Phys.* **201**, 100–112 (2017)
6. A. Abdelghany, E. Abdelrazek, S. Badr, M. Morsi, Effect of gamma-irradiation on (PEO/PVP)/Au nanocomposite: materials for electrochemical and optical applications. *Mater. Design* **97**, 532–543 (2016)
7. E.M. Abdelrazek, I.S. Elashmawi, A.M. Hezma et al., Effect of an encapsulate carbon nanotubes (CNTs) on structural and electrical properties of PU/PVC nanocomposites. *Physica B* **502**, 48–55 (2016)
8. A. Rajeh, M. Morsi, I.S. Elashmawi, Enhancement of spectroscopic, thermal, electrical and morphological properties of polyethylene oxide/carboxymethyl cellulose blends: combined FT-IR/DFT. *Vacuum* **159**, 430–440 (2019)
9. W.H. Eisa, Y.K. Abdel-Moneam, A. Shabaka, A.E.M. Hosam, In situ approach induced growth of highly monodispersed Ag nanoparticles within free standing PVA/PVP films. *Spectrochim. Acta A* **95**, 341–346 (2012)
10. M. Morsi, M. Abdelaziz, A.H. Oraby, I. Mokhles, Structural, optical, thermal, and dielectric properties of polyethylene oxide/carboxymethyl cellulose blend filled with barium titanate. *J. Phys. Chem. Solids* **125**, 103–114 (2019)
11. N.H. El Fewaty, A. El Sayed, R. Hafez, Synthesis, structural and optical properties of tin oxide nanoparticles and its CMC/PEG-PVA nanocomposite films. *Polym. Sci. A* **58**(6), 1004–1016 (2016)
12. M. El-Bana, G. Mohammed, A.M. El Sayed, S. El-Gamal, Preparation and characterization of PbO/carboxymethyl cellulose/polyvinylpyrrolidone nanocomposite films. *Polym. Compos.* **39**, 3712–3725 (2017)
13. M. Morsi, M. Abdelaziz, A. Oraby, I. Mokhles, Effect of lithium titanate nanoparticles on the structural, optical, thermal and electrical properties of polyethylene oxide/carboxymethyl cellulose blend. *J. Mater. Sci.: Mater. Electron.* **29**(18), 15912–15925 (2018)
14. E. Abdelrazek, A. Abdelghany, S. Badr, M. Morsi, Morphological, thermal and electrical properties of (PEO/PVP)/Au nanocomposite before and after gamma-irradiation. *J. Res. Updates Polym. Sci.* **6**(2), 45–54 (2017)
15. F.A. El-Kader, N. Hakeem, I. Elashmawi, A. Menazea, Synthesis and characterization of PVK/AgNPs nanocomposites prepared by laser ablation. *Spectrochim. Acta A* **138**, 331–339 (2015)
16. M. Mendivil, S. Shaji, G. Castillo, B. Krishnan, Transmission electron microscopic studies on noble metal nanoparticles

- synthesized by pulsed laser ablation in liquid. In *Microscopy: advances in scientific research and education center*, 1st edn, ed. by A. Méndez-Vilas (Formatex Research Center, 2014), pp. 911–920
17. M.I. Mendivil Palma, B. Krishnan, G.A.C. Rodriguez, T.K. Das Roy, D.A. Avellaneda, S. Shaji, Synthesis and properties of platinum nanoparticles by pulsed laser ablation in liquid. *J. Nanomater.* (2016). <https://doi.org/10.1155/2016/9651637>
 18. J.P. Goud, M.S. Alkathy, K. Sandeep, S. Ramakanth, K.J. Raju, Influence of laser fluence on structural, optical and microwave dielectric properties of pulsed laser deposited Ba_{0.6}Sr_{0.4}TiO₃ thin films. *J. Mater. Sci.: Mater. Electron.* **29**(18), 15973–15982 (2018)
 19. D. Garza, G.G. García, M.M. Palma, D. Avellaneda, G. Castillo, T.D. Roy, B. Krishnan, S. Shaji, Nanoparticles of antimony sulfide by pulsed laser ablation in liquid media. *J. Mater. Sci.* **48**(18), 6445–6453 (2013)
 20. B. Gupta, R. Agarwal, M. Sarwar Alam, Preparation and characterization of polyvinyl alcohol-polyethylene oxide-carboxymethyl cellulose blend membranes. *J. Appl. Polym. Sci.* **127**(2), 1301–1308 (2013)
 21. A.M. Hezma, I.S. Elashmawi, A. Rajeh, M. Kamal, Change spectroscopic, thermal and mechanical studies of PU/PVC blends. *Physica B* **495**, 4–10 (2016)
 22. M.S. Abdel-Aziz, A. Hezma, Spectroscopic and antibacterial evaluation of nano-hydroxapatite polyvinyl alcohol biocomposite doped with microbial-synthesized nanogold for biomedical applications. *Polym. Plast. Technol. Eng.* **52**(14), 1503–1509 (2013)
 23. A. Abdelghany, M.S. Mekhail, E. Abdelrazek, M. Aboud, Combined DFT/FTIR structural studies of monodispersed PVP/Gold and silver nano particles. *J. Alloy. Compd.* **646**, 326–332 (2015)
 24. A.Y. Yassin, A.-R. Mohamed, E.M. Abdelrazek, M.A. Morsi, A.M. Abdelghany, Structural investigation and enhancement of optical, electrical and thermal properties of poly (vinyl chloride-co-vinyl acetate-co-2-hydroxypropyl acrylate)/graphene oxide nanocomposites. *J. Mater. Res. Technol.* (2018). <https://doi.org/10.1016/j.jmrt.2018.08.005>
 25. A. Abdelghany, E. Abdelrazek, A. Oraby, M. Morsi, Role of LiBr inorganic filler on physical properties of polyether sulfone thermoplastic polymer. *Quantum Matter* **5**(2), 233–242 (2016)
 26. E. Abdelrazek, I. Elashmawi, Characterization and physical properties of CoCl₂ filled polyethyl-methacrylate films. *Polym. Compos.* **29**(9), 1036–1043 (2008)
 27. M. Wang, L. Xu, H. Hu, M. Zhai, J. Peng, Y. Nho, J. Li, G. Wei, Radiation synthesis of PVP/CMC hydrogels as wound dressing. *Nucl. Instrum. Methods Phys. Res. B* **265**(1), 385–389 (2007)
 28. K.K. Kumar, M. Ravi, Y. Pavani, S. Bhavani, A. Sharma, V.V.R.N. Rao, Investigations on PEO/PVP/NaBr complexed polymer blend electrolytes for electrochemical cell applications. *J. Membr. Sci.* **454**, 200–211 (2014)
 29. K.N. Kumar, K. Sivaiah, S. Buddhudu, Structural, thermal and optical properties of Tb³⁺, Eu³⁺ and co-doped (Tb³⁺+Eu³⁺): PEO + PVP polymer films. *J. Lumin.* **147**, 316–323 (2014)
 30. K. Kumar, M. Ravi, Y. Pavani, S. Bhavani, A. Sharma, V.V.R.N. Rao, Electrical conduction mechanism in NaCl complexed PEO/PVP polymer blend electrolytes. *J. Non-Cryst. Solids* **358**(23), 3205–3211 (2012)
 31. A. Abdelghany, E. Abdelrazek, D. Rashad, Impact of in situ preparation of CdS filled PVP nano-composite. *Spectrochim. Acta A* **130**, 302–308 (2014)
 32. H. Wang, X. Qiao, J. Chen, X. Wang, S. Ding, Mechanisms of PVP in the preparation of silver nanoparticles. *Mater. Chem. Phys.* **94**(2), 449–453 (2005)
 33. A. Hebeish, M. El-Rafie, F. Abdel-Mohdy, E. Abdel-Halim, H.E. Emam, Carboxymethyl cellulose for green synthesis and stabilization of silver nanoparticles. *Carbohydr. Polym.* **82**(3), 933–941 (2010)
 34. A. Hebeish, M. Hashem, M.A. El-Hady, S. Sharaf, Development of CMC hydrogels loaded with silver nano-particles for medical applications. *Carbohydr. Polym.* **92**(1), 407–413 (2013)
 35. R.P. Chahal, S. Mahendia, A. Tomar, S. Kumar, γ -Irradiated PVA/Ag nanocomposite films: materials for optical applications. *J. Alloy. Compd.* **538**, 212–219 (2012)
 36. N. Misra, J. Biswal, A. Gupta, J. Sainis, S. Sabharwal, Gamma radiation induced synthesis of gold nanoparticles in aqueous polyvinyl pyrrolidone solution and its application for hydrogen peroxide estimation. *Radiat. Phys. Chem.* **81**(2), 195–200 (2012)
 37. A.D. Dwivedi, K. Gopal, Biosynthesis of silver and gold nanoparticles using *Chenopodium album* leaf extract. *Colloids Surf. A* **369**(1), 27–33 (2010)
 38. D. Zhang, B. Gökce, S. Barcikowski, Laser synthesis and processing of colloids: fundamentals and applications. *Chem. Rev.* **117**(5), 3990–4103 (2017)
 39. D. Zhang, B. Gökce, Perspective of laser-prototyping nanoparticle-polymer composites. *Appl. Surf. Sci.* **392**, 991–1003 (2017)
 40. Y. Liu, S. Chen, L. Zhong, G. Wu, Preparation of high-stable silver nanoparticle dispersion by using sodium alginate as a stabilizer under gamma radiation. *Radiat. Phys. Chem.* **78**(4), 251–255 (2009)
 41. W.H. Eisa, Y.K. Abdel-Moneam, Y. Shaaban, A.A. Abdel-Fattah, A.M.A. Zeid, Gamma-irradiation assisted seeded growth of Ag nanoparticles within PVA matrix. *Mater. Chem. Phys.* **128**(1–2), 109–113 (2011)
 42. T. Tsuji, Y. Okazaki, M. Tsuji, Photo-induced morphological conversions of silver nanoparticles prepared using laser ablation in water-Enhanced morphological conversions using halogen etching. *J. Photochem. Photobiol. A* **194**(2), 247–253 (2008)
 43. K. Nouneh, M. Oyama, G. Lakshminarayana, I. Kityk, A. Wojciechowski, K. Ozga, Kinetics of picosecond laser treatment of silver nanoparticles on ITO substrate. *J. Alloys Compd.* **509**(40), 9663–9668 (2011)
 44. M. Noruzi, D. Zare, K. Khoshnevisan, D. Davoodi, Rapid green synthesis of gold nanoparticles using *Rosa hybrida* petal extract at room temperature. *Spectrochim. Acta A* **79**(5), 1461–1465 (2011)
 45. G. Mohammed, A.M. El Sayed, W. Morsi, Spectroscopic, thermal, and electrical properties of MgO/polyvinyl pyrrolidone/polyvinyl alcohol nanocomposites. *J. Phys. Chem. Solids* **115**, 238–247 (2017)
 46. S. El-Sayed, K. Mahmoud, A. Fatah, A. Hassen, DSC, TGA and dielectric properties of carboxymethyl cellulose/polyvinyl alcohol blends. *Physica B* **406**(21), 4068–4076 (2011)
 47. B. Ghanbarzadeh, H. Almasi, Physical properties of edible emulsified films based on carboxymethyl cellulose and oleic acid. *Int. J. Biol. Macromol.* **48**(1), 44–49 (2011)
 48. A. Goswami, A. Bajpai, J. Bajpai, B. Sinha, Designing vanadium pentoxide-carboxymethyl cellulose/polyvinyl alcohol-based bio-nanocomposite films and study of their structure, topography, mechanical, electrical and optical behavior. *Polym. Bull.* **75**(2), 781–807 (2018)
 49. A. Saroj, R. Singh, S. Chandra, Thermal, vibrational, and dielectric studies on PVP/LiBF₄ + ionic liquid [EMIM][BF₄]-based polymer electrolyte films. *J. Phys. Chem. Solids* **75**(7), 849–857 (2014)
 50. C. Lii, P. Tomasik, H. Zaleska, S. Liaw, V.M.F. Lai, Carboxymethyl cellulose-gelatin complexes. *Carbohydr. Polym.* **50**(1), 19–26 (2002)
 51. W. Tongdeesontorn, L.J. Mauer, S. Wongruong, P. Sriburi, P. Rachtanapun, Effect of carboxymethyl cellulose concentration on physical properties of biodegradable cassava starch-based films. *Chem. Cent. J.* **5**(1), 6–13 (2011)
 52. E. Gimeno, C. Moraru, J. Kokini, Effect of xanthan gum and CMC on the structure and texture of corn flour pellets expanded by microwave heating. *Cereal Chem.* **81**(1), 100–107 (2004)

53. S. Mir, T. Yasin, H.M. Siddiqi, G. Murtaza, Thermal, rheological, mechanical and morphological behavior of high density polyethylene and carboxymethyl cellulose blend. *J. Polym. Environ.* **25**(4), 1011–1020 (2017)
54. E. Abdelrazek, I. Elashmawi, S. Labeeb, Chitosan filler effects on the experimental characterization, spectroscopic investigation and thermal studies of PVA/PVP blend films. *Physica B* **405**(8), 2021–2027 (2010)
55. J.-F. Su, Z. Huang, X.-Y. Yuan, X.-Y. Wang, M. Li, Structure and properties of carboxymethyl cellulose/soy protein isolate blend edible films crosslinked by Maillard reactions. *Carbohydr. Polym.* **79**(1), 145–153 (2010)
56. M. Loría-Bastarrachea, W. Herrera-Kao, J. Cauich-Rodríguez, J. Cervantes-Uc, H. Vázquez-Torres, A. Ávila-Ortega, A TG/FTIR study on the thermal degradation of poly (vinyl pyrrolidone). *J. Therm. Anal. Calorim.* **104**(2), 737–742 (2011)
57. E.M. Abdelrazek, A.M. Abdelghany, S.I. Badr, M.A. Morsi, Structural, optical, morphological and thermal properties of PEO/PVP blend containing different concentrations of biosynthesized Au nanoparticles. *J. Mater. Res. Technol.* **7**(4), 419–431 (2018)